APS physics

CHORUS

This is the accepted manuscript made available via CHORUS. The article has been published as:

# Exploring the high-pressure behavior of superhard tungsten tetraboride

Miao Xie, Reza Mohammadi, Zhu Mao, Matt M. Armentrout, Abby Kavner, Richard B. Kaner, and Sarah H. Tolbert

Phys. Rev. B **85**, 064118 — Published 24 February 2012

DOI: 10.1103/PhysRevB.85.064118

# Exploring the High Pressure Behavior of Superhard Tungsten Tetraboride

Miao Xie,[1] Reza Mohammadi,[1,3] Zhu Mao,[4] Matt M. Armentrout,[4] Abby Kavner,[4,*]
Richard B. Kaner,[1,2,3,*] and Sarah H. Tolbert[1,2,3,*]

[1]*Department of Chemistry and Biochemistry, University of California, Los Angeles, CA 90095, USA*
[2]*California NanoSystems Institute (CNSI), University of California, Los Angeles, CA 90095 USA*
[3]*Department of Materials Science and Engineering, University of California, Los Angeles, CA 90095, USA*
[4]*Department of Earth and Space Sciences and Institute of Geophysics and Planetary Physics, University of California, Los Angeles, CA 90095, USA*

[*]Corresponding authors: tolbert@chem.ucla.edu, kaner@chem.ucla.edu, akavner@ucla.edu

**Abstract:** In this work, we examine the high pressure behavior of superhard material candidate $WB_4$ using high-pressure synchrotron X-ray diffraction in a diamond anvil cell up to 58.4 GPa. The zero-pressure bulk modulus, $K_0$, obtained from fitting the pressure-volume data using the second-order Birch-Murnaghan equation of state is 326 ± 3 GPa. A reversible, discontinuous change in slope in the *c/a* ratio is further observed at ~42 GPa, suggesting that lattice softening occurs in the *c* direction above this pressure. This softening is not observed in other superhard transition metal borides such as $ReB_2$ compressed to similar pressures. Speculation on the possible relationship between this softening and the orientation of boron-boron bonds in the *c* direction in the $WB_4$ structure is included. Finally, the shear and Young's modulus values are calculated using an isotropic model based on the measured bulk modulus and an estimated Poisson's ratio for $WB_4$.

*Keywords*: Bulk modulus; Hardness; High pressure; Rhenium diborde, Second-order phase transition; Superhard, Tungsten tetraboride; Ultra-incompressible; X-ray diffraction.

## I. INTRODUCTION

The search for new superhard materials is driven by the need for chemically-inert robust materials for abrasives, cutting tools, and coatings that can be synthesized under modest conditions. Broadly, two approaches are used to design and synthesize materials with high hardness. A first approach is to imitate natural diamond by combining light first row elements (B, C, N or O) to produce materials that maintain short bonds with high-covalency, such as *c*-BN,[1] $B_6O$,[2] and $BC_2N$.[3] A second route is to start with elemental metals that are intrinsically incompressible, but not hard, and try to improve their hardness by incorporating light elements into the metal structure to simultaneously optimize covalent bonding and valence-electron density.[4] This class, which generally contains late, transition-metal borides, carbides, nitrides, and oxides contains many candidate hard materials.[5-8]

For example, by applying the second approach to Os, with a hardness of only 3.9 GPa, Cumberland *et al.*[9] sought to introduce covalent bonds to its lattice using boron to increase its hardness while maintaining the high bulk modulus. The presence of covalent bonds in $OsB_2$ results in a hardness of 21.6 GPa under an applied load of 0.49 N, without substantially reducing the bulk modulus (365-395 GPa).[9,10] Although this hardness value is relatively high, it does not assign this material to the "superhard" category.[11] One reason for this is that the $OsB_2$ structure contains double Os layers, alternating with covalent B layers. The weak Os-Os metallic bonds within the layers likely reduce the resistance of $OsB_2$ to large shear deformations in the easy-slip direction, which is parallel to the layers.[11] To create potentially harder materials, hexagonal rhenium diboride was synthesized by completely replacing Re for Os. The $ReB_2$ structure consists of alternating single layers of hexagonally-packed Re and puckered interconnected hexagonal rings of boron. Without the double metal layers that

reduced the hardness for $OsB_2$, this material exhibits a much higher hardness of 48 ± 5.6 GPa under an applied load of 0.49 N.[12]

The next logical step in this pattern would be to further increase the boron concentration in a related late transition metal boride to further increase the hardness. Unfortunately, few transition metals form compounds with boron to metal ratios greater than 2:1. Tungsten, however, is an exception, forming the unusual compound tungsten tetraboride ($WB_4$). It is the highest boride formed under normal pressures.[13-15] Interestingly, the structure of $WB_4$ exhibits a unique covalent bonding network with B-B covalent bonds aligned along the *c*-axis.[16] This covalent bonding framework of $WB_4$ should result in a more isotropic structure than that exhibited by $ReB_2$. In general, isotropic structures favor high hardness, as demonstrated in diamond, because materials fail at the weakest point. This suggests that $WB_4$, embracing a more isotropic structure, has potential for improved hardness. As a candidate superhard material, $WB_4$ also has a number of advantages over other borides. Specifically, 1) both tungsten and boron are relatively inexpensive, 2) the lower metal content in the higher borides reduces the overall cost per volume of production and 3) the higher boron content lowers the overall density of the compound, which could prove to be beneficial in applications where light-weight is a critical asset.[17]

Recently, Gu *et al*.[18] synthesized $WB_4$ and they measured hardness values as high as 46.2 GPa and a bulk modulus of 304 ± 10 GPa by fitting the second-order Birch-Murnaghan equation of state (EOS). With an exceptionally-high first derivative $K_0'$ of 15.3 ± 5.7, they obtained an extremely low value of the zero pressure bulk modulus $K_0$ of 200 ± 40 GPa using the third-order Birch-Murnaghan equation of state. Unfortunately, this work did not include any details on the synthesis of the $WB_4$ or present any raw X-ray diffraction data; thus, it is

difficult to effectively evaluate the lattice behavior of $WB_4$ from this work, especially under extreme conditions. In parallel, Wang *et al.*[16] theoretically predicted the hardness of $WB_4$ to be between 41.1-42.2 GPa with a bulk modulus of 292.7-324.3 GPa. They also calculated a low shear modulus of 103.6-181.6 GPa. More recently, Liu *et al.*[19] studied the high pressure behavior of $WB_4$ synthesized using a hot press and compressed to 50.8 GPa with silicone oil as the pressure medium. The authors obtained values ranging from 256 to 342 GPa, depending on the equation of state and the pressure range. Changing the pressure range can have a significant effect with silicone oil, because this pressure medium has a hydrostatic limit of 8 GPa,[20] and develops a deviatoric stress of 1 GPa at pressures as low as 10 GPa.[21] Non-hydrostaticity can result in strongly biased determination of elastic properties, and also can result in diffraction peak broadening and loss of resolution that may mask small changes in the lattice parameter that indicate structural transitions. Thus, our current study aims to examine lattice behavior of $WB_4$ under more hydrosatic conditions, with a goal of resolving these conflicts in the value of bulk modulus.

In our recent study, high-quality crystalline $WB_4$ was successfully synthesized via arc melting. We confirmed the high hardness using both microindentation and nanoindentation, obtaining hardness values of 43.3 ± 2.9 GPa, and 40.4 GPa, respectively.[17] From high pressure X-ray diffraction results, a bulk modulus of 339 ± 3 GPa was obtained using a second order finite strain EOS. This value was 10% higher than the value reported by Gu *et al.*[18] and was close to some of the value reported by Liu *et al.*[19]

In order to clarify the elastic moduli of $WB_4$ with higher accuracy and to further examine the lattice distortions of $WB_4$ under elevated pressure, we have undertaken a more complete experimental study of the pressure-dependent compression behavior of $WB_4$ using

synchrotron-based angle-dispersive X-ray diffraction in the diamond anvil cell. It is now widely recognized that hydrostaticity is the key to obtaining reliable values of bulk modulus and its pressure derivatives, particularly for fairly incompressible materials. We have thus used neon as pressure transmitting medium since it offers good quasihydrostatic conditions to at least 50 GPa.[20] In addition, we have performed a similar set of experiments on $ReB_2$ to 63 GPa, allowing us to compare and contrast the behavior of these two transition metal borides. The example of $ReB_2$ provides a good cross-comparison because of the close proximity of Re to W in the periodic table, the similar valence electron densities of these two materials ($ReB_2$: 0.477 $e^-Å^{-3}$; $WB_4$: 0.485 $e^-Å^{-3}$), the similar indentation hardness values measured for these materials (48.0 ± 5.6 GPa and 43.3 ± 2.9 GPa for $ReB_2$[12] and $WB_4$[17], respectively), and their related structure (both space group *$P6_3/mmc$*).

## II. EXPERIMENTAL PROCEDURE

Powders of pure tungsten (99.9994%, JMC Puratronic, USA) and amorphous boron (99+%, Strem Chemicals, USA) were mixed together with a molar ratio of 1:11 and pressed into a pellet using a Carver press under 10,000 lbs. of force. The pellets were then placed in an arc melting furnace. The $WB_4$ ingot was synthesized by applying an AC current of >70 amps under high-purity argon at ambient pressure. All ingots were crushed to form a fine powder using a hardened-steel mortar and pestle set. The rhenium diboride sample was produced in a two step process that involved first synthesizing $ReB_2$ powder and then sintering the powder into an ingot. The detailed description of the process can be found elsewhere.[22] To confirm the phase purity of all powder samples, powder X-ray diffraction patterns were collected on an X'Pert Pro™ X-ray powder diffraction system (PANalytical, Netherlands) (Fig. 1). Elemental analysis was performed using a JSM-6700F field-emission scanning electron

microscopy (JEOL Ltd.) equipped with an energy-dispersive X-ray spectroscopy detector (EDAX) utilizing an ultrathin window.

High-pressure experiments were carried out using a symmetric diamond anvil cell equipped with 300 μm diamond culets using a pre-indented rhenium gasket with a 150 μm diameter sample chamber. A 50 μm diameter piece of sample was loaded into the cell, supported by a piece of platinum foil (5 μm thick, 99.95%, Alfa Aesar, USA), which was as an internal pressure calibrant. We also placed a 10 μm ruby chip next to the sample as an external pressure calibrant. To ensure a quasi-hydrostatic sample environment, neon gas was loaded into the cell using the COMPRES/GSECARS gas loading system.[23] High-pressure angle dispersive X-ray diffraction experiments were performed at Beamline 12.2.2 at the Advanced Light Source (ALS, Lawrence Berkeley National Laboratory) and 16-BM-D of the HPCAT sector of the Advanced Photon Source (APS) with X-ray beam sizes of approximately 10 ×10 $\mu m^2$ and 5 ×15 $\mu m^2$, respectively. Image plate detectors were used at both beamlines. The distance and orientation of the detector were calibrated using $LaB_6$ and $CeO_2$ standards, respectively. Pressure was determined using ruby fluorescence. A secondary pressure calibration was performed by referencing the measured lattice parameter of the internal standard Pt to its P-V equation of state. X-ray diffraction patterns of $WB_4$ and $ReB_2$ were collected up to pressures of 58.4 and 63 GPa, respectively.

## III. RESULTS

At ambient temperature and pressure, X-ray diffraction studies of $WB_4$ reveal a hexagonal structure with the lattice parameters $a$ = 5.1945 ± 0.0013 Å, $c$ = 6.3311 ± 0.0030 Å, $V_0$ = 147.94 ± 0.15 $Å^3$ and axial ratio $c/a$ = 1.2188 ± 0.0006 (Fig. 1). Representative high-pressure diffraction patterns for $WB_4$ are shown in Fig. 2. The two-dimensional diffraction patterns

were integrated using the program FIT2D[24] to yield one-dimensional plots of X-ray intensity as a function of *d*-spacing. All patterns were indexed to the hexagonal phase, and there were no signs of phase transformations. The sample remained in the hexagonal phase up to the highest pressure of 58.4 GPa, at which point the lattice parameters were $a = 4.949 \pm 0.013$ Å and $c = 5.984 \pm 0.027$ Å and $V_0 = 126.9 \pm 1.30$ Å$^3$. Similarly, $ReB_2$ was also shown to be stable in the hexagonal phase to 63 GPa.

Figure 3 shows the normalized unit cell volume of $WB_4$ as a function of pressure, under both compression (filled circles) and decompression (open circles). Figure 4 shows the normalized compressibility of both the *a*- and *c*-lattice parameters of $WB_4$. Up to ~40 GPa, both the *a*- and *c*-lattice constants show a gentle decrease upon compression, with the *a*-axis appearing slightly more compressible than the *c*-axis. However, at ~42 GPa, the *c*-axis appears to suddenly undergo a softening, becoming significantly more compressible than the *a*-axis. The *a*-axis does not show any change in behavior. This structural change is reversible, with the *c*-lattice constant recovering its original strain values upon decompression. This structural change has not been observed in other studies and emphasizes the need for high-quality data.

Due to this anomalous behavior in the *c* direction, fits to the Birch-Murnaghan equation of state were performed at pressures lower than 42 GPa. The measured zero-pressure bulk modulus, $K_0$, using a second-order Birch-Murnaghan equation of state is 317 ± 3 GPa. Using a third-order Birch-Murnaghan equation of state, we obtain values of $K_0 = 367 \pm 11$ GPa and $K_0' = 0.9 \pm 0.6$. Using only data obtained on compression results in $K_0 = 326 \pm 3$ GPa (second-order Birch-Murnaghan equation of state) and $K_0 = 369 \pm 9$ GPa with $K_0' = 1.2 \pm 0.5$ (third-order Birch-Murnaghan equation of state). The second order values are slightly lower than our previous study of $WB_4$, which presented a bulk modulus of 339 ± 3 GPa obtained

using a second-order finite strain equation of state.[17] The inferred values of $K_0$ and $(dK/dP)_0$ are strongly correlated, however, with an inverse relationship. For the $WB_4$ data up to 40 GPa, the pairs ($K_0$, $K_0'$) = (326, 4) and (369, 1.2) are statistically indistinguishable. The trade-offs between the two parameters are plotted in Fig. 6, which shows contours for the sum of the deviations from the fits as a function of varying $K_0$ and $K_0'$. The trade-off between $K_0$ and $K_0'$ produces a change in bulk modulus of -12 GPa for every 1 of $K_0'$ $WB_4$. This relationship is sufficient to explain the variation in previous studies, including the exceptional low bulk modulus in Gu's results.[18]

Figure 3 also shows the compression and decompression behavior of $ReB_2$ up to 63 GPa. Second-order Birch-Murnaghan equation fitting to the $ReB_2$ data gives an ambient bulk modulus of $K_0$ = 344 ± 1 GPa, with a similar trade-off between $K_0$ and $(dK/dP)_0$ (Fig. 6). The measured bulk modulus is slightly lower than the previously-reported bulk modulus of 360 GPa, also obtained using second-order Birch-Murnaghan equation of state fits to pressure-dependent X-ray diffraction,[12] but both values fall in the range of 317-383 GPa previously reported from resonant ultrasound spectroscopy (RUS) experiments (Table I).[22, 25-29] Fitting the third-order Birch-Murnaghan equation of state gives $K_0$ = 340 ± 5 GPa with $K_0'$ = 4.2 ± 0.2. Compressibility along different crystallographic axes in hexagonal $ReB_2$ is illustrated in Fig. 5. Importantly, close examination of *a*- and *c*-lattice constants shows no evidence of lattice softening in either direction. Comparison of Fig. 4 and 5 also clearly emphasizes the fact that $WB_4$ shows much more isotropic bonding than $ReB_2$ with much more similar compressibility in *a* and *c* directions.

## III. DISCUSSION

At the point of the structural change at 42 GPa, the $WB_4$ diffraction pattern remains the same, with no evidence of peak broadening or splitting (Fig. 2). Thus, there is no evidence for a first-order phase transition. Additionally, the compression behavior is reversible upon release of pressure. Since this transition pressure for $WB_4$ (42 GPa) appears far from the hydrostatic limit of the pressure medium (~15 GPa),[20] it is unlikely that deviation from hydrostaticity is responsible for this observation. Additionally, if deviatoric stresses were affecting the measured X-ray strains, the axial geometry of the X-ray in the diamond anvil cell combined with the gasket direction would predict the opposite observation—that lattice planes should appear less compressible, not more compressible, as the medium becomes less hydrostatic. As a result, it appears that the abrupt change in *c/a* ratio observed at 42 GPa is a real structural change of the system; specifically, a second-order phase transition. The challenge now is to understand the origins of this phase transition and to determine if it can provide insight into the bonding found in this unique metal tetraboride.

To make a more direct comparison between the high-pressure behavior of $WB_4$ and $ReB_2$, we examined their *c/a* ratios normalized to each other at ambient pressure. Because the unit cells are not the same in these two materials, the absolute *c/a* ratios are rather different (1.2188 for $WB_4$ and 2.5786 for $ReB_2$) (Fig. 7). Normalization is thus required to compare the fairly small changes observed here. Up to ~40 GPa, both materials show a linear increase in their *c/a* ratio of similar magnitude. However, this increase continues for $ReB_2$ while there is a discontinuous change in slope for the *c/a* ratio at ~42 GPa for $WB_4$. As shown in Fig. 4, this *c/a* ratio drop can be almost solely accounted for by the anomalous compression behavior of the *c*-axis.

This structural change may be mechanical or may be electronic in nature. Electronic band structure calculations has been reported on $ReB_2$ without any evidence for transitions up to 90 GPa,[30] but less is known for $WB_4$. While transitions based on changes in optimal atomic positions or bond orientation may seem to be the likely explanation for the observed transitions, other anomalous compression phenomena have been documented experimentally[31-34] and theoretically[35-43] when distortion of the electronic band structure results in a topological singularity of the Fermi surface. Those are known as electronic topological transitions (ETTs) or Lifshitz transitions.[44] The anomaly has mostly been found in hcp metals including Zn,[31-34] Cd,[31] and Os,[46,47] and intermetallic compound such as $AuIn_2$,[42, 43] or $Cd_{0.8}Hg_{0.2}$.[45] However, these transitions are highly controversial because of their subtle nature and because of difficulties in their direct experimental detection at high pressures. The magnitude of the anomalies observed in the compression data associated with ETTs is usually small, as opposed to the significant softening observed in $WB_4$. In addition, most of the discontinuities associated with electronic phase transition occur below 20 GPa (e.g. calculated to be 7 and 14 GPa for Zn;[40] observed at 2.7 GPa for $AuIn_2$[42, 43]). Moreover, ETTs do not necessarily affect only one lattice direction and usually result in a decrease in compressibility after the anomaly. While the possibility of an ETT in $WB_4$ at high pressure is intriguing, the data do not fit the standard profile for these transitions, and thus it seems likely that the observed bond softening in $WB_4$ does not arise from this kind of singularity, but is instead due to changes in optimal bonding at high pressure.

Lacking the observation of peak splitting and/or a new phase in the X-ray diffraction data, we assign this anomaly to a structurally-induced second-order phase transition. The intersection of the two regions defines the transition pressure at 42 GPa. Furthermore, Fig. 7 reveals that although the *c/a* compression behavior is reversible, the *c/a* ratio does not fully recover its

compression value until the pressure is decreased to less than 20 GPa. Such hysteresis further indicates that the softening is mechanical, rather than electronic in origin.

In order to understand this decompression behavior, the nature of the second-order phase transition of $WB_4$, and the lack of similar pressure-induced lattice-axis softening in $ReB_2$ and $OsB_2$, it is essential to consider the crystal structures of both $ReB_2$ and $WB_4$ (Fig. 8(a) and (b)). The crystal structure of $ReB_2$ (Fig. 8(a)) is characterized by alternating layers of metal atoms and boron atoms. The boron atoms are condensed into six-membered rings in a chair-like conformation. The Re atoms are arranged in a hexagonal close-packed layer with B atoms occupying all tetrahedral voids; this enlarges the lattice by about 40%. A strong anisotropy has been found in the hexagonal structure (Fig. 5), with the *c*-axis much less compressible than the *a*-axis. This can be explained by the directional electronic repulsion between the borons and transition metal atoms aligned along the *c*-axis. This repulsion reduces the pressure induced compression in the *c* direction. Because the layers are not highly constrained in the *a*-*b* direction, continuous structural optimization upon compression results in smooth and continuous changes in the *c*-axis lattice constant up to 63 GPa.

The most widely cited structure of $WB_4$ was originally assigned by Romans and Krug in 1966,[13] which consists of alternating layers of hexagonal network of boron and hexagonal layers of tungsten atoms (Fig. 8(b)). In contrast with the $ReB_2$ structure (Fig. 8(a)), however, these planar B layers are propped up by B-B bonds aligned along the *c*-axis. This could make the *c* direction more compressible (pure B is more compressible than $ReB_2$) and less flexible. We hypothesize that because of the more constrained bonding in the $WB_4$ structure, high-pressure bond optimization within the ambient-pressure structure may be difficult and a second-order phase transition could be required to optimize the bonding at high pressure.

This would not be the case for the less constrained $ReB_2$ structure, which shows no signs of phase transitions up to 63 GPa. Upon decompression, the structural distortion is recovered, but rather incomplete at a low pressure, as is typical for pressure-induced phase transitions.

Note that at least one competing, although lesser known, structure has been proposed for $WB_4$ (Fig. 8(c)).[48] While the tungsten lattice remains the same, there are considerable stoichiometric variations ($WB_4$ *vs.* $W_{1.83}B_9$) and boron lattice dissimilarities between the two structures. The unresolved structure certainly warrants more investigation, but for this discussion, the differences may not be that important as both structures contain a three-dimensional boron network, including both boron layers in the *a*-*b* plane and boron covalent bonding in the *c* direction.

Because the primary interest in both $ReB_2$ and $WB_4$ is for applications as hard materials, the structural insights gained by examining lattice behavior under high-pressure conditions may be used to establish design parameters for developing new superhard materials. In order for a solid to have a high hardness, it must possess sufficient structural integrity that can survive large shear strains without collapse.[49] A strongly covalently-bonded three-dimensional and isotropic network may ensure high intrinsic hardness of a material, as seen in diamond and *c*-BN.[50] In $WB_4$, the presence of strong covalent B-B bonds in the *c*-axis apparently adds three-dimensional rigidity to the structure, which could reduce the chances of shear deformation, or the creation and motion of the dislocations. At the same time, this three-dimensional boron bonding could create a more isotropic bonding environment that can potentially withstand larger shear strains.

Moreover, high-pressure X-ray absorption spectroscopy on $ReB_2$ has shown flattening of the boron layers with increasing hydrostatic pressures.[51] The flattening should facilitate slipping of the layers in the *a*-*b* plane and further reduce the hardness under load. Therefore, it may be that $WB_4$ possesses a higher resistance to shear strain and less dislocation activity compared to $ReB_2$ because of its three-dimensional, almost isotropic covalently-bonded network. Although $WB_4$ is more compressible than $ReB_2$, it is intrinsically as hard, if not harder, than $ReB_2$. While the pressure-induced bond softening observed here is not a cause of this increased hardness; it is likely that the structural change observed in $WB_4$, but not in $ReB_2$, and the comparatively high hardness of $WB_4$ both stem from the increased stiffness of $WB_4$ that arises from the three-dimensional boron network.

Many attempts have been made to correlate hardness with other physical properties for a wide range of hard materials, especially bulk modulus and shear modulus.[4,9,12,29,52-65] Shear modulus is generally a much better predictor of hardness than bulk modulus.[52-58] We thus present here a calculated shear modulus of $WB_4$, obtained from the bulk modulus and an estimated Poisson's ratio using an isotropic model. We begin the estimation by assuming $WB_4$ has little elastic anisotropy, as demonstrated in $OsB_2$[27] and $ReB_2$,[28] so that an isotropic model can be applied. Since the Poisson's ratio of $WB_4$ has not yet been experimentally measured, the recently-reported value of 0.1958 for $ReB_2$ from resonant ultrasound spectroscopy is used.[26] An isotropic model is then applied to estimate the shear modulus and the Young's modulus based on the measured bulk modulus and estimated Poisson's ratio of $WB_4$. The calculated shear and Young's modulus values are compared with first-principles calculations and nanoindentation data in Table I. The measured bulk modulus (326 GPa) is in excellent agreement with the first-principles calculations based on the LDA method (324 GPa)[16] and falls between Gu *et al.*[18] and our previous X-ray diffraction data.[17] Our shear

modulus derived from the isotropic model is 249 GPa, comparable with the measured shear modulus of $ReB_2$ (223-276 GPa)[22, 25] and nearly twice the value reported from theoretical calculations (104-129 GPa).[16] Although many assumptions went into calculating this shear modulus, the high value seems reasonable given the similar hardnesses of $ReB_2$ and $WB_4$, and the known correlation between shear modulus and hardness. Finally, the Young's modulus calculated from the bulk modulus in a similar manner to the shear modulus is 595 GPa, which is only slightly higher than the value of 553.8 GPa derived from nanoindentation measurements,[17] but lower than the measured Young's modulus of $ReB_2$ (642-671 GPa).[29]

## V. CONCLUSIONS

$WB_4$ and $ReB_2$ were studied using synchrotron X-ray diffraction under quasihydrostatic conditions up to 58.4 and 63 GPa, respectively. In contrast to $ReB_2$, we found an anomalous lattice softening of the *c*-axis in $WB_4$ during compression, which was partially reversible during decompression. The anomaly was assigned to a second-order phase transition and may be due to pressure-induced structural rearrangements that are required because of the more rigid nature of the $WB_4$ network, compared with $ReB_2$. We believe that the three-dimensional, almost isotropic, rigid covalently boron network in $WB_4$ is responsible for both the observed structural change in $WB_4$ and its high intrinsic hardness. In addition, based on our measured bulk modulus and an estimated Poisson's ratio, a high shear modulus of 249 GPa was estimated for $WB_4$ using an isotropic model.

By examining the behavior of superhard materials like $WB_4$ under extreme conditions such as highly-elevated pressures, we begin to understand the structural change that take place in these strongly-bonded solids. In this way, we build up a knowledge base so that future

iterations of ultra-incompressile superhard materials can be produced by design, rather than by the trial-and-error process that we are often forced to employ.

## ACKNOWLEDGEMENTS

The authors thank Andrew T. Lech and Beth E. Weaver for their assistance in experiments. This work was funded by the National Science Foundation under grants DMR-0805357 and DMR-1106364 (SHT and RBK). Portions of this work were performed at the Advanced Light Source, Lawrence Berkeley National Laboratory. The Advanced Light Source is supported by the Director, Office of Science, Office of Basic Energy Sciences, of the U.S. Department of Energy under Contract No. DE-AC02-05CH11231. Portions of this work were performed at HPCAT (Sector 16) and GeoSoilEnviroCARS (Sector 13), Advanced Photon Source (APS), Argonne National Laboratory. HPCAT is supported by DOE-BES, DOE-NNSA, NSF, and the W.M. Keck Foundation. GeoSoilEnviroCARS is supported by the National Science Foundation - Earth Sciences (EAR-0622171) and Department of Energy-Geosciences (DE-FG02-94ER14466). APS is supported by DOE-BES, under Contract No. DE-AC02-06CH11357.

## REFERENCES

[1]T. Taniguchi, M. Akaishi, and S. Yamaoka, J. Am. Ceram. Soc. **79**, 547 (1996).

[2]D. W. He, Y. S. Zhao, L. Daemen, J. Qian, T. D. Shen, and T. W. Zerda, Appl. Phys. Lett. **82**, 643 (2002).

[3]V. L. Solozhenko, D. Andrault, G. Fiquet, M. Mezouar, and D. C.Rubie, Appl. Phys. Lett. **78**, 1385 (2001).

[4]R. B. Kaner, J. J. Gilman, and S. H. Tolbert, Science **308**, 1268 (2005).

[5]J. S. Tse, D. D. Klug, K. Uehara, Z. Q. Li, J. Haines, and J. M. Léger, Phys. Rev. B **61**, 10029 (2000).

[6]H. C. Lee and J. Gurland, Mater. Sci. Eng. **33**, 125 (1978).

[7]A. Zerr, G. Miehe, and R. Riedel, Nat. Mater. **2**, 185 (2003).

[8]D. S. Stone, K. B. Yoder, and W. D. Sproul, J. Vac. Sci. Technol. A **9**, 2543 (1991).

[9]R. W. Cumberland, M. B. Weinberger, J. J. Gilman, S. M. Clark, S. H. Tolbert, and R. B. Kaner, J. Am. Chem. Soc. **127**, 7264 (2005).

[10]H.-Y. Chung, J. M. Yang, S. H. Tolbert, and R. B. Kaner, J. Mater. Res. **23**, 1797 (2008).

[11]J. Yang, H. Sun, and C. Chen, J. Am. Chem. Soc. **130**, 7200 (2008).

[12]H.-Y. Chung, M. B. Weinberger, J. B. Levine, A. Kavner, J.-M. Yang, S. H. Tolbert, and R. B. Kaner, Science **316**, 436 (2007).

[13]P. A. Romans and M. P. Krug, Acta Cryst. **20**, 313 (1996).

[14]L. G. Bodrova, M. S. Kovalchenko, and T. I. Serebryakova, Powder Metall. Met. C+ **13**, 1 (1974).

[15]H. Itoh, T. Matsudaira, S. Naka, H. Hamamoto, and M. Obayashi, J. Mater. Sci. **22**, 2811 (1987).

[16]M. Wang, Y. Li, T. Cui, Y. Ma, and G. Zou, Appl. Phy. Lett. **93**, 101905 (2008).

[17]R. Mohammadi, A. T. Lech, M. Xie, B. E. Weaver, M. T. Yeung, S. H. Tolbert, and R. B. Kaner, Proc. Nat. Acad. Sci. **108**, 10959 (2011).

[18]Q. Gu, G. Krauss, and W. Steurer, Adv, Mater. **20**, 3630 (2008).

[19]C. Liu, F. Peng, N, Tan, J. Liu, F. Lia, J. Qin, J. Wang, Q. Wang, and D. He, High Press. Res. **31**, 2 (2011).

[20]S. Klotz, J.-C. Chervin, P. Munsch, and G. Le Marchand, J. Phys. D: Appl. Phys. **42**, 075413 (2009).

[21]J. Zhao, R. J. Angel and N. L. Ross, J. Appl. Cryt. **43**, 743 (2010).

[22]J. B. Levine, J. B. Betts, J. D. Garrett, S. Q. Guo, J. T. Eng, A. Migliori, and R. B. Kaner, Acta Materialia **58**, 1530 (2010).

[23]M. Rivers, V. B. Prakapenka, A. Kubo, C. Pullins, C. M. Holl, and S. D. Jacobsen, High Press. Res. **28**, 273 (2008).

[24]A. Hammersley, S. Svensson, M. Hanfland, A. Fitch, and D. Hausermann, High Press. Res. **14**, 235 (1996).

[25]M. R. Koehler, V. Keppens, B. C. Sales, R. Y. Jin, and D. Mandrus, J. Phys. D **42**, 095414 (2009).

[26]Y. Suzukia, J. B. Levine, A. Migliori, J. D. Garrett, R. B. Kaner, V. R. Fanelli, and J. B. Betts, J. Acoust. Soc. Am. **127**, 2797 (2010).

[27]Y. X. Wang, Appl. Phys. Lett. **91**, 101904 (2007).

[28]X. F. Hao, Y. H. Xu, Z. J. Wu, D. F. Zhou, X. J. Liu, X. Q. Cao, and J. Meng, Phys. Rev. B **74**, 224112 (2006).

[29]H.-Y. Chung, M. B. Weinberger, J. M. Yang, S. H. Tolbert, and R. B. Kaner, Appl. Phys. Lett. **92**, 261904 (2008).

[30]E. Zhao, J. Wang, J. Meng, and Z. Wu, J. Comput. Chem. **31**, 1904 (2010).

[31]K. Takemura, Phys. Rev. B **56**, 5170 (1997).

[32]K. Takemura, Phys. Rev. Lett. **75**, 1807 (1995).

[33]O. Schulte and W.B. Holzapfel, Phys. Rev. B **53**, 569 (1996).

[34]K. Takemura, Phys. Rev. B **60**, 6171 (1999).

[35]S. Meenakshi, V. Vijayakumar, B.K. Godwal, and S.K. Sikka, Phys. Rev. B **46**, 14359 (1992).

[36]B.K. Godwal, S. Meenakshi, and R.S. Rao, Phys. Rev. B **56**, 14871 (1997).

[37]D. L. Novikov, M. I. Katnelson, A. V. Trefilov, A. J. Freeman, N. E. Christensen, A. Svane, and, C. O. Rodriguez, Phys. Rev. B **59**, 4557 (1999).

[38]G. S-Neumann, L. Stixrude, and R.E. Cohen, Phys. Rev. B **63**, 54103 (2001).

[39]B. K. Godwal, P. Modak, and R. S. Rao, Solid State Commun. **125**, 401 (2003).

[40]S. L. Qiu, F. Apostol, and P. M. Marcus, J. Phys.: Condens. Matter **16**, 6405 (2004).

[41]G. V. Sin'ko and N. A. Smirnov, J. Phys.: Condens. Matter **17**, 559 (2005).

[42]B. K. Godwal, A. Jayaraman, S. Meenakshi, R. S. Rao, S. K. Sikka, and V. Vijayakumar, Phys. Rev. B **57**, 773 (1998).

[43]B. K. Godwal, S. Speziale, S. M. Clark, J. Yan, and R. Jeanloz, J. Phys. Chem. Solids **71**, 1059 (2010).

[44]I. M. Lifshitz, Sov. Phys. JETP **11**, 1130 (1960).

[45]S. Speziale, R. Jeanloz, S. M. Clark, S. Meenakshi, V. Vijayakumar, A. K. Verma, R. S. Rao, and B. K. Godwal, J. Phys. Chem. Solids **69**, 2325 (2008).

[46]F. Occelli, D. L. Farber, J. Badro, C. M. Aracne, D. M. Teter, M. Hanfland, B. Canny, and B. Couzinet, Phys. Rev. Lett. **93**, 095502 (2004).

[47]D. Koudela, M. Richter, A. Möbius, K. Koepernik, and H. Eschrig, Phy. Rev. B **74**, 214103 (2006).

[48]H. Nowotny, H. Haschke, and F. Benesovsky, Monatsh. Chem. **98**, 547 (1967).

[49]S. Veprek, A. S. Argon, and R. F. Zhang, Philosophical Magazine **90**, 4101 (2010).

[50]S. Veprek, J. Vac. Sci. Technol. A **17**, 2401 (1999).

[51]J. Pellicer-Porres, A. Segura, A. Muñoz, A. Polian, and A. Congeduti, J. Phys.: Condens. Matter **22**, 045701 (2010).

[52]J. J. Gilman, R. W. Cumberland, and R. B. Kaner, Int. J. Refract. Met. Hard Mater. **24**, 1 (2006).

[53]V. V. Brazhkin, A. G. Lyapin, and R. J. Hemley, Philos. Mag. A **82**, 231 (2001).

[54]N. Dubrovinskaia, L. Dubrovinsky, W. Crichton, F. Langenhorst, and A. Richter, Appl. Phys. Lett. **87**, 831061 (2005).

[55]N. Dubrovinskaia, L. Dubrovinsky, and V. L. Solozhenko, Science **318**, 1550c (2007).

[56]J. S. Tse, J. Superhard Mater. **32**, 177 (2010).

[57]A.P. Gerk, J. Mater. Sci. **12**, 735 (1977).

[58]D.M. Teter, MRS Bull. **23**, 22 (1998).

[59]J. J. Gilman, *Electronic Basis of the Strength of Materials* (Cambridge University Press, Cambridge, 2003).

[60]C. M. Sung and M. Sung, Mater. Chem. Phys. **43**, 1 (1996).

[61]J. Haines, J. M. Leger, and G. Bocquillon, Annu. Rev. Mater. Res. **31**, 1 (2001).

[62]J. M. Leger, J. Haines, M. Schmidt, J. P. Petitet, A. S. Pereira, and J. A. H. Dajornada, Nature (London) **383**, 401 (1996).

[63]A. Y. Liu and M. L. Cohen, Science **245**, 841 (1989).

[64]V. V. Brazhkin, A. G. Lyapin, and R. J. Hemley, Philos. Mag. A **82**, 231 (2002).

[65]A. R. Oganov and A. O. Lyakhova, J. Superhard Mater. **32**, 143 (2010).

**FIGURES**

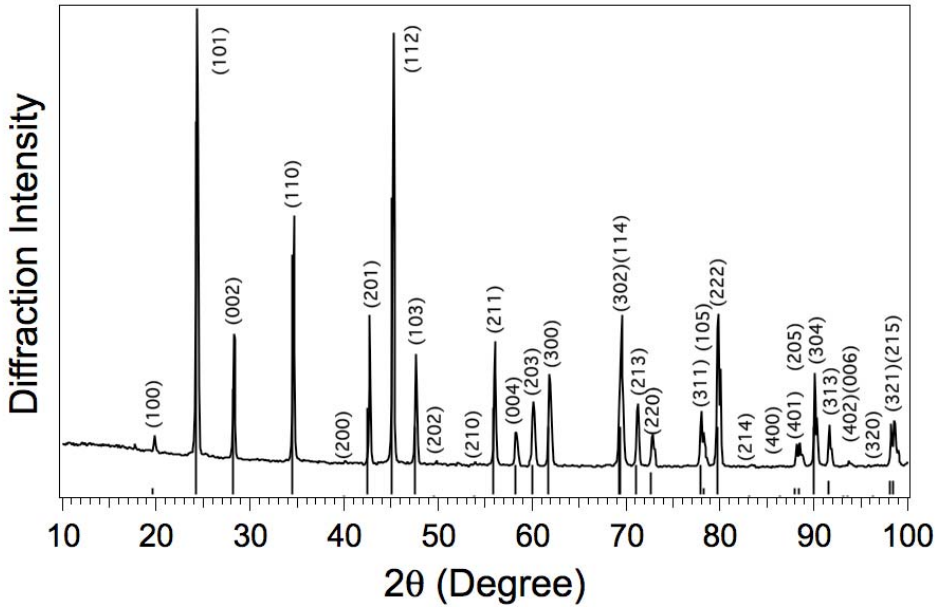


**FIG. 1.** Labeled X-ray diffraction pattern for powder tungsten tetraboride ($WB_4$) at ambient pressure (X-ray wavelength $\lambda$ = 1.54 Å). The vertical bars indicate previously determined lattice spacings for $WB_4$ (JCPDS, Ref. Code: 00-019-1373).[13] The corresponding Miller index is given above each peak. The material used in this work is thus shown to be highly crystalline and phase pure.

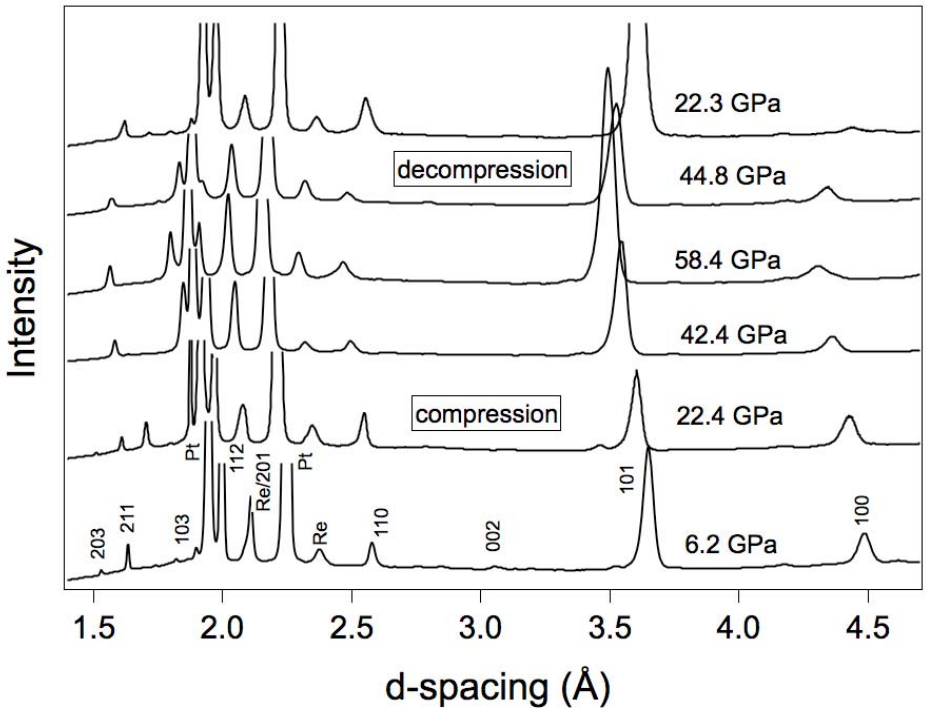


**FIG. 2.** Representative angle dispersive X-ray diffraction patterns for $WB_4$ as a function of increasing and decreasing pressure. The Re peaks are from the gasket due to incomplete filtering of the tails of the X-ray beam. No changes in peak patterns that would be indicative of a change in symmetry are observed under pressures up to 58.4 GPa.

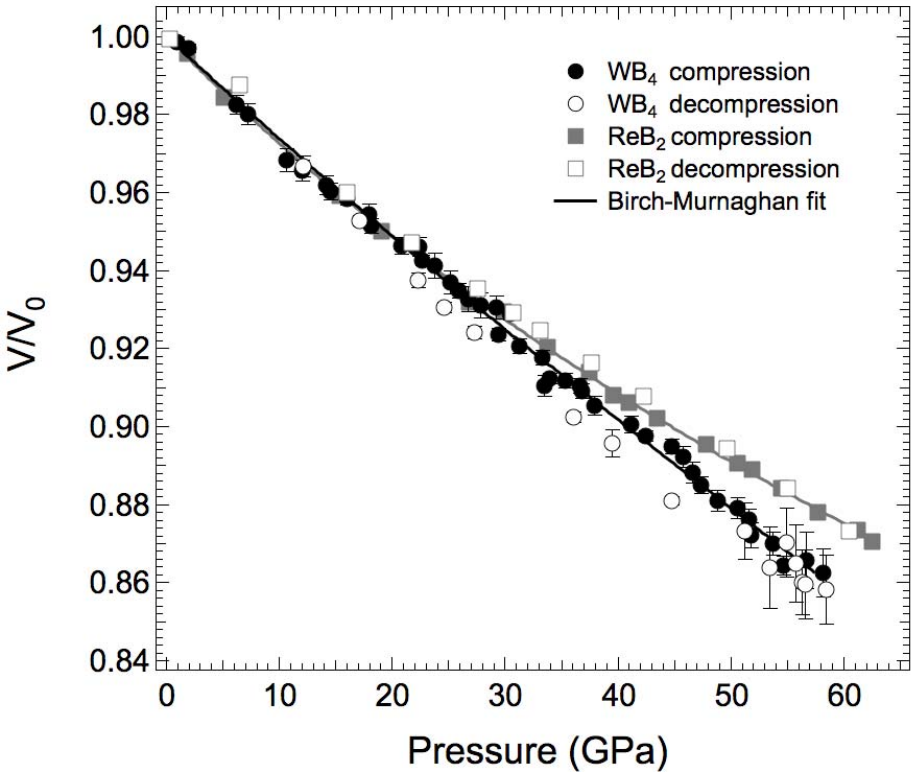


**FIG. 3.** Measured fractional unit cell volume of $WB_4$ and $ReB_2$ plotted as a function of pressure. Black solid circle: compression of $WB_4$; black open circle: decompression of $WB_4$; grey solid square: compression of $ReB_2$; grey open square: decompression of $ReB_2$; black solid line: a Birch-Murnaghan fit to the compression data of $WB_4$; grey solid line: a Birch-Murnaghan fit to the compression data of $ReB_2$. Error bars that are smaller than the size of the symbol have been omitted. While $WB_4$ is more compressible than $ReB_2$ under high pressures, below 30 GPa the data are quite comparable.

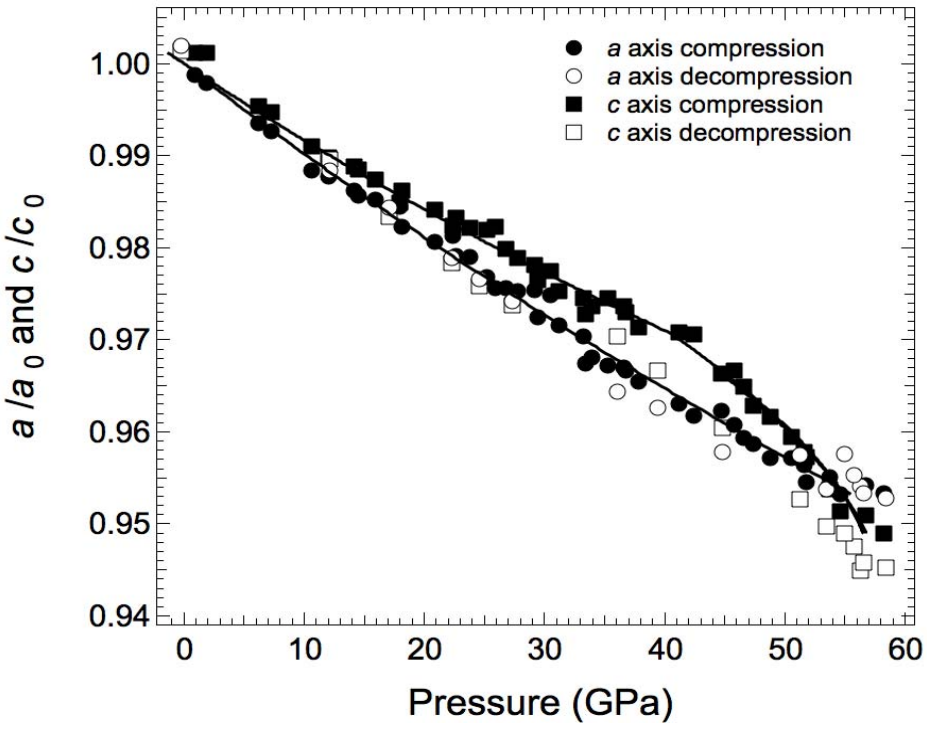


**FIG. 4.** $WB_4$ fractional lattice parameters plotted as a function of pressure. Black solid circles: compression data for the *a*-lattice constant; black open circle: decompression data for the *a*-lattice constant; black solid squares: compression data for the *c*-lattice constant: black open square: decompression for the *c*-lattice constant; solid lines: fits to the Birch-Murnaghan equation of state. The error bars when not shown are smaller than the symbol. At ~42 GPa during compression, the *c*-lattice constant undergoes a softening and becomes more compressible than the *a*-lattice constant. The *a*-lattice constant does not exhibit this abrupt change. Decompression data reveals that this structural change is reversible, but with some hysteresis.

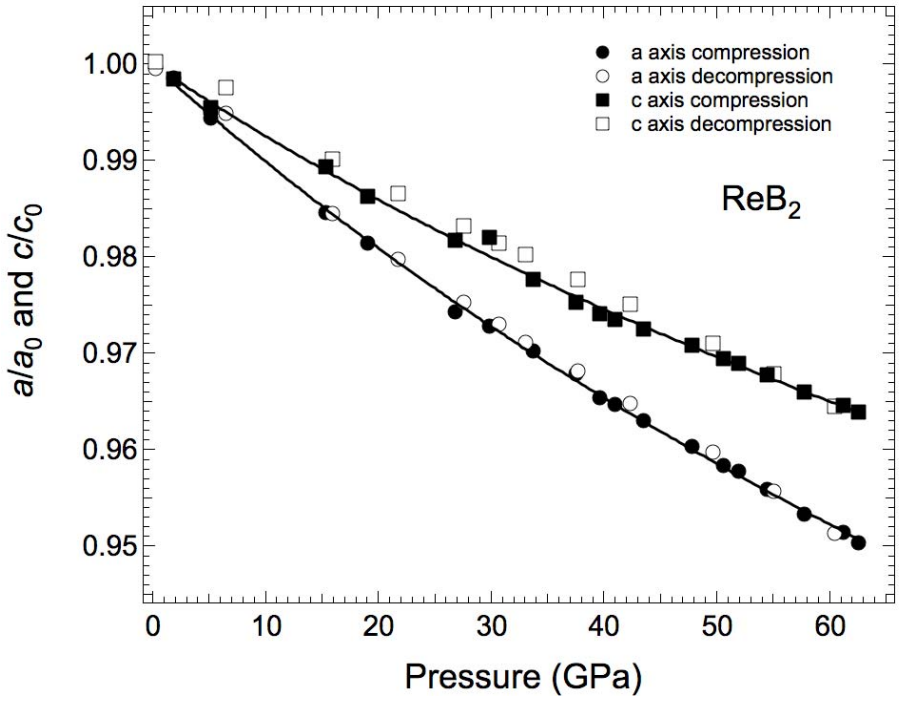


**FIG. 5.** $ReB_2$ fractional lattice parameters plotted as a function of pressure Black solid circles: compression data for the *a*-lattice constant; black open circle: decompression data for the *a*-lattice constant; black solid squares: compression data for the *c*-lattice constant: black open square: decompression for the *c*-lattice constant; solid lines: fits to the Birch-Murnaghan equation of state. Examination of the *a*- and *c*-lattice constants shows no evidence of lattice softening in either direction during compression.

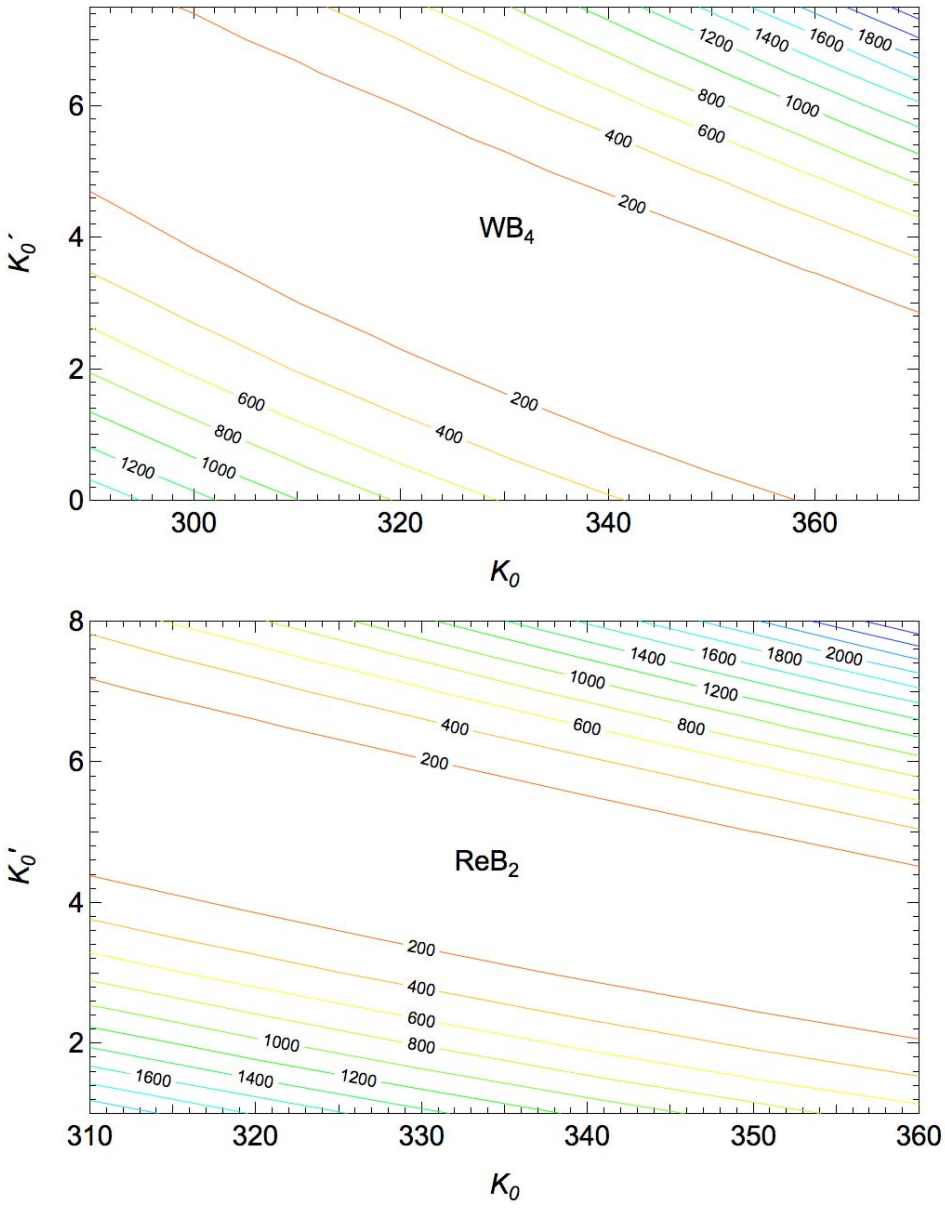


**FIG. 6.** (Color online) Tradeoff of zero-pressure bulk modulus $K_0$ and its first derivative $K_0'$ for $WB_4$ and $ReB_2$. The contours are the sum of the deviations from the fits as a function of varying $K_0$ and $K_0'$. The inferred values of $K_0$ and $K_0'$ have an inverse relationship. The value obtained from second or third order Birch-Murnaghan equation of state cannot be statistically distinguished based on this analysis.

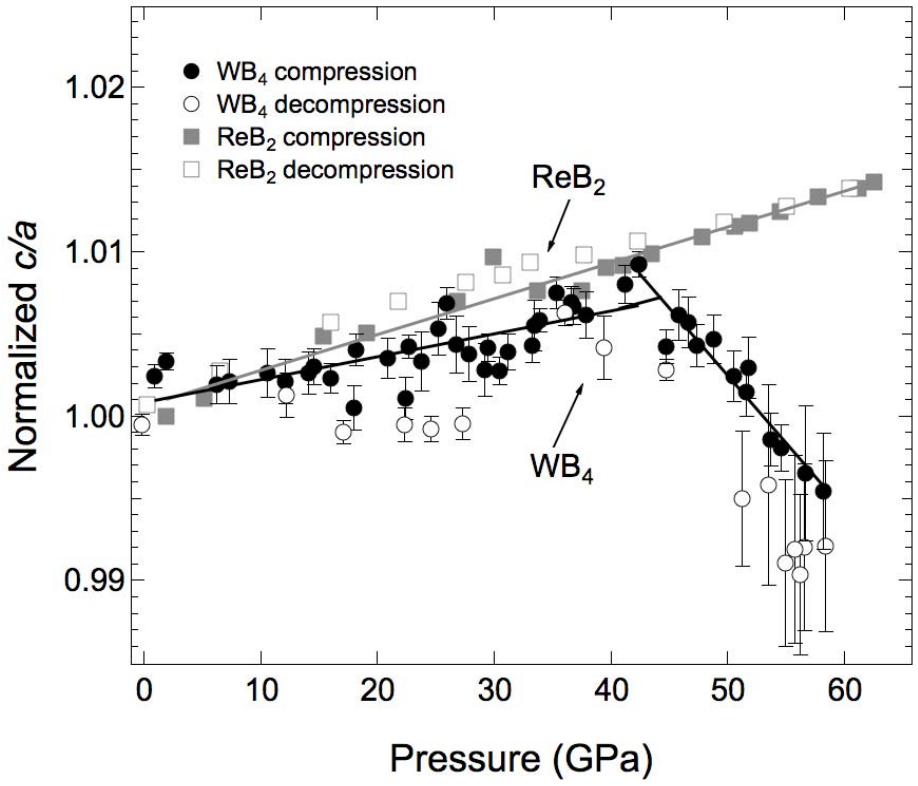


**FIG. 7.** Normalized *c/a* ratio plotted as a function of pressure for $WB_4$ and $ReB_2$. Black solid circle: compression of $WB_4$; black open circle: decompression of $WB_4$; grey solid square: compression of $ReB_2$; grey open square: decompression of $ReB_2$; solid lines: linear fits of compression data serve as a guide to the eye. $WB_4$ undergoes a pressure-induced second-order phase transition at ~42 GPa. This transition is reversible with some hysteresis, suggesting a mechanical origin. In contrast, $ReB_2$ shows no evidence of a phase transition. The different pressure behavior can be related to difference in crystal structures between these two materials.

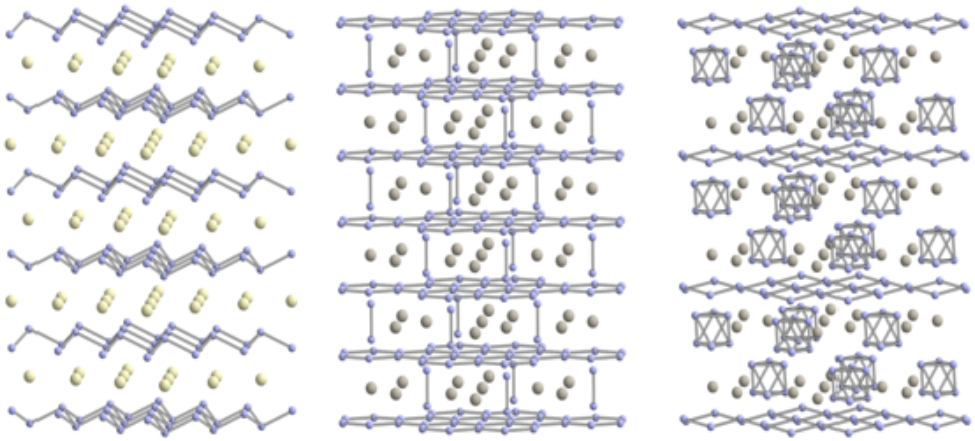

(a) (b) (c)

**FIG. 8.** (Color online) (a) Crystal structure of $ReB_2$; (b) suggested structure of $WB_4$ and (c) a second suggested structure for $WB_4$ ($W_{1.83}B_9$). The presence of the boron-boron covalent bonds in $WB_4$ may account for its distinct high pressure behavior relative to $ReB_2$.

**TABLE I.** Comparison of the theoretical calculations and experimental results for the bulk modulus $K_0$ (GPa) and their first derivative $K_0'$, shear modulus $G$ (GPa), Young's modulus $E$ (GPa), Poisson's ratio $\nu$ of $WB_4$ and $ReB_2$ found in the literature and presented in this study

| Material | | | $K_0$ | $K_0'$ | $G$ | $E$ | $\nu$ |
|---|---|---|---|---|---|---|---|
| $ReB_2$ | Cal. | Wang *et al.* (LDA)[27] | 359 | | 313 | 696 | 0.22 |
| | | Wang *et al.* (GGA)[27] | 344 | | 304 | 642 | 0.21 |
| | | Hao *et al.* (LDA)[28] | 369.2 | | 294.9 | 698.7 | 0.1846 |
| | | Hao *et al.* (GGA)[28] | 354.5 | | 289.4 | 682.5 | 0.1791 |
| | Expt. | Chung *et al.* (X-ray)[12] | 360[a] | 4 | | 712[29] | |
| | | Levine *et al.* (RUS)[22] | 383[b] | | 273 | 661 | 0.21 |
| | | Koehler *et al.* (RUS)[25] | 317[b] | | 276 | 642 | 0.163 |
| | | Suzuki *et al.* (RUS)[26] | 367.7[b] | | 271.6 | 671.2 | 0.1958 |
| | | This work | 344[a] | 4 | | | |
| | | | 340[a] | 4.2 | | | |
| $WB_4$ | Cal. | Wang *et al.* (GGA)[16] | 292.7 | | 103.6 | | |
| | | Wang *et al.* (LDA)[16] | 324.3 | | 129.1 | | |
| | Expt. | Mohammadi *et al.*[17] (X-ray) | 339[a] | 4 | | 553.8 | |
| | | Gu *et al.*[18] (X-ray) | 304[a] | 4 | | | |
| | | | 200[a] | 15.3 | | | |
| | | Liu *et al.*[19] (X-ray) | 342[a] | 4 | | | |
| | | | 325[a] | 5.1 | | | |
| | | This work | 326[a] | 4 | 249 | 595 | |
| | | | 369[a] | 1.2 | | | |

[a]Reported bulk modulus $K_0$ are isothermal values. Measured bulk modulus is obtained by fitting Birch-Murnaghan equation of state.
[b]Reported bulk moduli are adiabatic values.